GEOPHYSICS, VOL. 52, NO. 7 (JULY 1987); P. 943–964, 20 FIGS.

A new slant on seismic imaging: Migration and integral geometry

In contrast, the classical diffraction stack always provides a [illegible] tial from its projections, i.e., from seismic data. The problem of

are surfaces in model space that come from fixing a point $\mathbf{d} = (\mathbf{r}, \mathbf{s}, t)$ in the data and finding the surface of image points

sponding pair of projection operators (Miller, 1983):

medium, so that

$$\nabla^2 G_0(\mathbf{x}, \mathbf{y}, \omega) + \frac{\omega^2}{c_0^2(\mathbf{x})} G_0(\mathbf{x}, \mathbf{y}, \omega) = -\delta(\mathbf{x} - \mathbf{y}). \quad (6)$$

With these definitions, equation (4) can be recast as an integral equation, analogous to the Lippman-Schwinger equation of quantum mechanics (see, e.g., Taylor, 1972),

$$u(\mathbf{y}, \mathbf{s}, \omega) = G_0(\mathbf{y}, \mathbf{s}, \omega) + \omega^2 \int d^3\mathbf{x}\; G_0(\mathbf{y}, \mathbf{x}, \omega) f(\mathbf{x}) u(\mathbf{x}, \mathbf{s}, \omega).$$

When evaluated at receiver position $\mathbf{r}$, this equation gives the observed total field as a sum of the incident field within the background model G_0 plus the scattered field, represented by the integral term. Denoting the scattered field by

$$\left[\nabla_{\mathbf{x}}\, \tau(\mathbf{x}, \mathbf{y})\right]^2 = c_0^{-2}(\mathbf{x}), \quad (9)$$

and the amplitude or geometrical spreading term A satisfies the transport equation

$$A(\mathbf{x}, \mathbf{y}) \nabla_{\mathbf{x}}\, \tau(\mathbf{x}, \mathbf{y}) 2 \nabla_{\mathbf{x}} A(\mathbf{x}, \mathbf{y}) \cdot \nabla_{\mathbf{x}'}(\mathbf{x}, \mathbf{y}) = 0, \quad (10)$$

along the ray connecting the points $\mathbf{x}$ and $\mathbf{y}$.

Substituting for G_0 in equation (8) gives

$$u_{sc}(\mathbf{r}, \mathbf{s}, \omega) = \omega^2 \int d^3\mathbf{x}\; A(\mathbf{r}, \mathbf{x}) A(\mathbf{x}, \mathbf{s}) \times \exp\left\{ i\omega \left[\tau(\mathbf{r}, \mathbf{x}) + \tau(\mathbf{x}, \mathbf{s}) \right] \right\} f(\mathbf{x})$$

$$= \omega^2 \int d^3\mathbf{x}\; A(\mathbf{r}, \mathbf{x}, \mathbf{s}) \exp\left[i\omega\tau(\mathbf{r}, \mathbf{x}, \mathbf{s}) \right] f(\mathbf{x}). \quad (11)$$

will contain a convolution with the source wavelet. One can then shift the time derivative onto the source wavelet itself (see Tarantola, 1984). For reasons explained in a later section, we keep these equations in the given form. In the final section, we briefly discuss the effect of a band limited source.

Analogy with the classical Radon transform

As **r**, **s**, and t vary over the data, the acoustic GRT gives weighted integrals of the scattering potential over isochron surfaces in the model. We derive an approximate inverse

[redacted]

formula (Radon, 1917; Gel'fand et al., 1966; Deans, 1983)

$$f(\mathbf{x}_0) = -\frac{1}{8\pi^2}\int d^2\xi \left[\frac{\partial^2}{\partial p^2} f^{\Delta}(\xi, p)\right]_{p=\xi\cdot\mathbf{x}_0}$$

$$= -\frac{1}{8\pi^2}\int d^2\xi \frac{\partial^2}{\partial p^2} f^{\Delta}(\xi, p = \xi\cdot\mathbf{x}_0). \qquad (16)$$

[redacted]

Equation (16) is the 3-D version of the filtered backprojection algorithm of X-ray tomography (see, e.g., Herman, 1980). For fixed ξ, the function $f^{\Delta}(\xi, p)$ is a one-dimensional function of p

[redacted]

equation (15), we can write for the filtered transform

$$\frac{\partial^2}{\partial p^2} f^{\Delta}(\xi, p) = \frac{\partial^2}{\partial p^2}\int d^3\mathbf{x}\, \delta(p - \xi\cdot\mathbf{x}) f(\mathbf{x})$$

$$= \int d^3\mathbf{x}\, \delta''(p - \xi\cdot\mathbf{x}) f(\mathbf{x}).$$

[redacted]

Combining this with equation (16) gives

$$f(\mathbf{x}_0) = -\frac{1}{8\pi^2}\int d^2\xi \int d^3\mathbf{x}\, \delta''\left[\xi\cdot(\mathbf{x}_0 - \mathbf{x})\right] f(\mathbf{x}). \qquad (17)$$

[redacted]

[redacted]

ing gives directly what may be called a "filtered" generalized Radon transform. To obtain the identification, first shift the

[redacted]

Consider first $\nabla_x \tau(\mathbf{r}, \mathbf{x}_0)$. Since rays are perpendicular to surfaces of equal traveltime (phase) and traveltime increases as $\mathbf{x}_0$ moves away from $\mathbf{r}$, this gradient points in the opposite direction from the ray that leaves $\mathbf{x}_0$ and reaches $\mathbf{r}$ in the background model, or along the ray that arrives at $\mathbf{x}_0$ from $\mathbf{r}$.

arrives at $\mathbf{x}_0$ from the source $\mathbf{s}$. The geometry is illustrated in Figure 6. We call these gradient vectors the incident and scattered rays at the image point $\mathbf{x}_0$.

From the eikonal equation (9), the magnitudes of the incident and scattered rays are equal to $1/c_0(\mathbf{x}_0)$, the slowness of the background model at the point $\mathbf{x}_0$. The total traveltime

gives the weighting function dW directly,

$$dW(\mathbf{r}, \mathbf{x}_0, \mathbf{s}) = \frac{1}{\pi^2} d^2\xi(\mathbf{r}, \mathbf{x}_0, \mathbf{s}) \frac{|\cos^3 \alpha(\mathbf{r}, \mathbf{x}_0, \mathbf{s})|}{c_0^3(\mathbf{x}_0) A(\mathbf{r}, \mathbf{x}_0, \mathbf{s})}, \quad (26)$$

and the final inversion formula

$$\langle f(\mathbf{x}_0) \rangle = \frac{1}{\pi^2} \int d^2\xi(\mathbf{r}, \mathbf{x}_0, \mathbf{s}) \times \frac{|\cos^3 \alpha(\mathbf{r}, \mathbf{x}_0, \mathbf{s})|}{c_0^3(\mathbf{x}_0) A(\mathbf{r}, \mathbf{x}_0, \mathbf{s})} u_{sc}(\mathbf{r}, \mathbf{s}, t = \tau_0). \quad (27)$$

The inversion integral we have derived is given explicitly in

The analysis described above carries through with only minor changes to yield the 2-D acoustic inversion formula

$$\langle f(\mathbf{x}_0)\rangle = \frac{1}{\pi}\int d\xi(\mathbf{r}, \mathbf{x}_0, \mathbf{s})$$

er here zero-offset and fixed-offset experiments in a constant background velocity. The zero-offset migration formula was first derived in Norton and Linzer (1981) by a different approach; the fixed-offset formula was derived in Beylkin (1985).

Zero-offset migration

factor $A(\mathbf{r}, \mathbf{x}, \mathbf{r}) = (4\pi|\mathbf{x}-\mathbf{r}|)^{-2}$ and substituting into equation (27) yields

$$\langle f(\mathbf{x})\rangle = \frac{16}{c_0^3}\int_{r_3=0} d^2\mathbf{r}\,\frac{x_3}{|\mathbf{x}-\mathbf{r}|}\,u_{sc}(\mathbf{r}, t = 2|\mathbf{x}-\mathbf{r}|/c_0)$$

$$= \frac{16}{c_0^3}\int d^2\mathbf{r}\,\cos\theta\, u_{sc}(\mathbf{r}, t = 2|\mathbf{x}-\mathbf{r}|/c_0). \quad (29)$$

[illegible]

A second algebraic derivation follows directly from equation (28). By definition, the surface integral

[illegible]

where the magnitude of the vector cross-product is the Jacobian factor. This again yields equation (29); moreover, if the data are collected on an irregular surface $r_3 = r_3(r_1, r_2)$, the only change in the derivation is that the third component of ξ becomes $x_3 - r_3(r_1, r_2)$. The latter construction works whenever it is possible to specify ξ explicitly in terms of the Cartesian coordinates of the experiment.

Fixed-offset experiments

Consider next a fixed-offset experiment on the surface of a half-space with constant background velocity. The experiment [illegible]

source-receiver pair. Let $\mathbf{h} = (h_1, h_2, 0)$ be the half-offset vector, so that the receiver position $\mathbf{r} = \mathbf{m} + \mathbf{h}$ and the source [illegible]

$$\xi = \frac{[illegible]}{\left[2 + (\mathbf{x}-\mathbf{s})\cdot(\mathbf{x}-\mathbf{r})/|\mathbf{x}-\mathbf{s}|\,|\mathbf{x}-\mathbf{s}|\right]^{1/2}} \times \left(\frac{\mathbf{x}-\mathbf{r}}{|\mathbf{x}-\mathbf{r}|} + \frac{\mathbf{x}-\mathbf{s}}{|\mathbf{x}-\mathbf{s}|}\right). \quad (31)$$

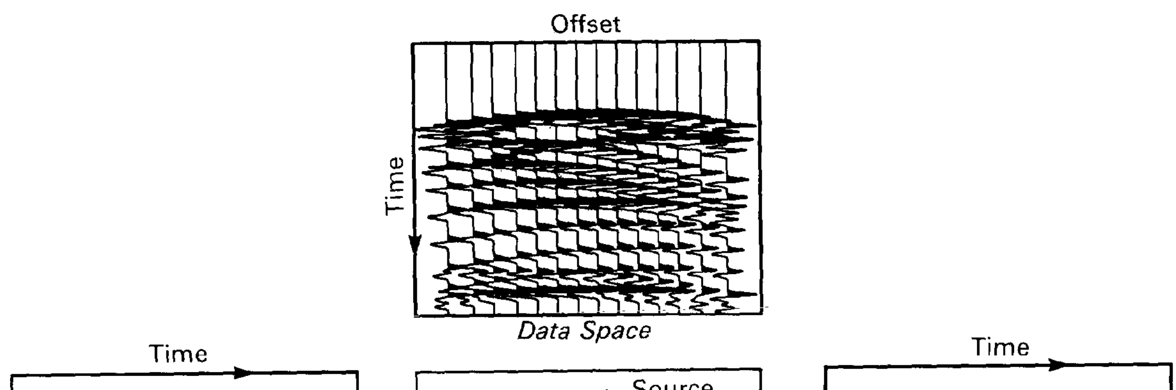

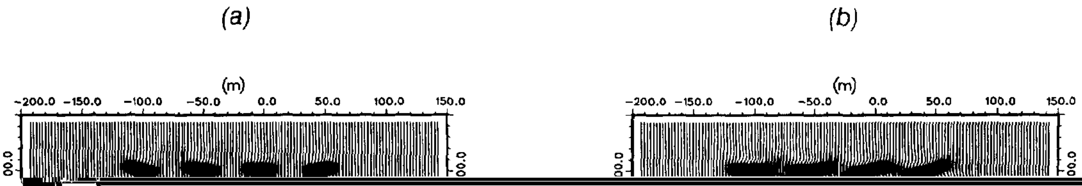
(a)
(b)
(m)
−200.0 −150.0 −100.0 −50.0 0.0 50.0 100.0 150.0
(m)
−200.0 −150.0 −100.0 −50.0 0.0 50.0 100.0 150.0

A change of variables can now be made from ξ to $\mathbf{m}$ using equations (30) and (31); however, the algebra is dense. For simplicity, consider the 2-D case and work with the angular variables defined in Figure 7; the polar angle θ determines ξ

source to the image point $\mathbf{x}$, and α_r is the angle between the vertical and the ray from the receiver to the image point $\mathbf{x}$. Then,

$$\theta = \frac{1}{2}(\alpha_s + \alpha_r) + \pi$$

$$= \frac{1}{2}\left(\tan^{-1}\frac{m-h}{z} + \tan^{-1}\frac{m+h}{z}\right) + \pi, \qquad (32)$$

in the scattering potential. Consider the velocity function defined by the relation

$$c^{-2}(z) = 1 + \Theta(z - z_0),$$

depth of the reflector. Taking $c_0^{-2} = 1$ gives the scattering potential

$$f(z) = \Theta(z - z_0).$$

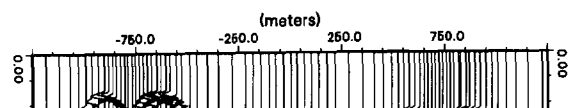

computed from integrals of [illegible] hemispheres. It follows from coverage of tangent planes passing through an image point;

faces, by setting the scattering potential to be

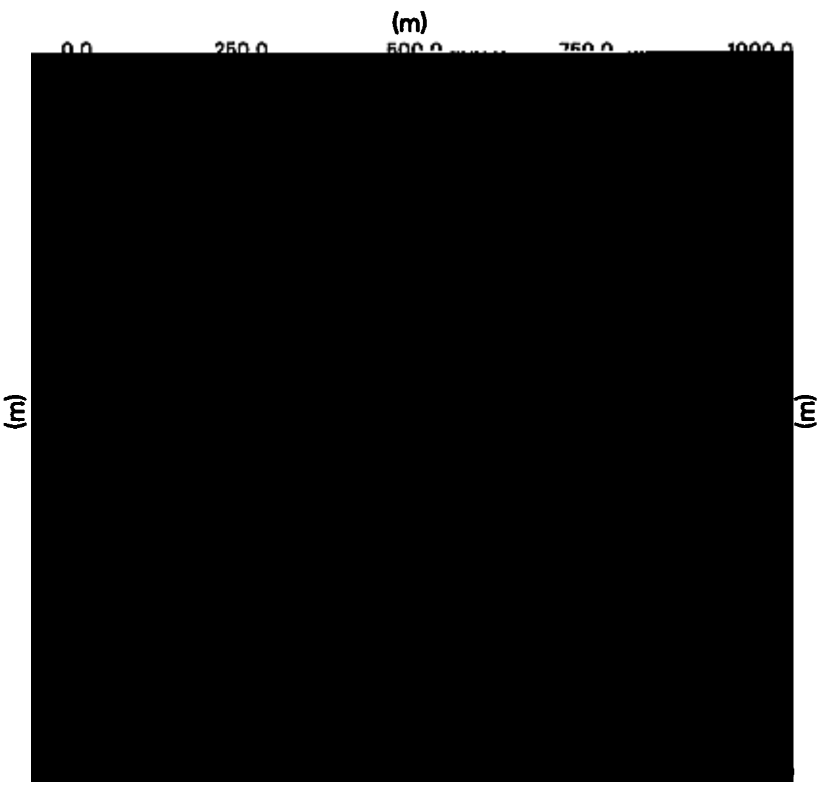

FIG. 15. Reconstruction from the synthetic DVSP experiment. (a) Ten wiggle plots showing profiles of the reconstruc- [redacted]

[redacted]

multiple-receiver experiment with the source and receivers arranged as in Figure 1. The scattering object consisted of a family of point scatterers, which were separated by roughly one wavelength at the central frequency of the source and

[redacted]

scattered data were obtained for 80 source-receiver pairs. The source wavelet was a Blackman-Harris window with a duration of 21.3 ms (which contains frequencies ranging from 0 to about 50 Hz).

[redacted]

mining the shapes and locations of the surfaces, the method is easily adapted to general source-receiver geometries and velocity models. Moreover, the dependence of spatial resolution on the geometry of the experiment, the reconstruction algorithm, and the assumptions about the medium is explicit in

perimental geometry and the finite bandwidth of the source wavelet.

The first issue is the relation between the available source-receiver pairs and the spatial dip spectrum of the reconstructed object. Locally, a restriction on the number of source

performing just surface experiments, just borehole experiments, or both. It is also possible to describe an ideal experi-

surfaces in the generalized Radon transform, and hence, the set of tangent planes (parameterized by ξ) available at each

[redacted]

$$\Delta p = \frac{c_0(\mathbf{x}_0)}{2\cos\alpha}\,\Delta t. \tag{36}$$

surface. This last figure illustrates the obliquity effect directly in the image domain.

The mapping of the data into the spatial Fourier spectrum


(sec.)
0.25
0.30
0.35
(m)
-75.0
-50.0
-25.0
0.0
25.0
50.0
75.0

borehole seismic profiles: A case study: Presented at the 55th Ann. Internat. Mtg., Soc. Explor. Geophys., Washington, D. C.,; abstracts and biographies 105–107.

Miller, D. E., 1983, Integral transforms and the migration of multiple-offset borehole seismic profiles: Research Note, Schlumberger-Doll Research.

Miller, D. E., and Dupal, L., 1986, Reef delineation by multiple offset

by its Fourier integral yielding

integrals which express these derivatives exist. For large ω